2010 IEEE International Conference on Robotics and Automation
Anchorage Convention District
May 3-8, 2010, Anchorage, Alaska, USA

Safe Joint Mechanism using Inclined Link with Springs for Collision Safety and Positioning Accuracy of a Robot Arm

Jung-Jun Park and Jae-Bok Song

Abstract—**In recent years, the potential for collision between humans and robots has drawn much attention since service robots are increasingly being used in the human environment. A safe robot arm can be achieved using either an active or passive compliance method. A passive compliance system composed of purely mechanical elements often provides faster and more reliable responses to dynamic collision than an active system involving sensors and actuators. Since positioning accuracy and collision safety of a robot arm are equally important, a robot arm should have very low stiffness when subjected to a collision force capable of causing human injury. Otherwise, it should maintain a very high stiffness. To implement these requirements, a novel safe joint mechanism (SJM-III) consisting of an inclined link, a slider with rollers, and linear springs is proposed. The SJM-III has the advantage of nonlinear stiffness, which can be achieved only with passive mechanical elements. Various analyses and experiments on static and dynamic collisions show high stiffness of the SJM-III against an external torque less than a predetermined threshold torque, with an abrupt drop in stiffness when the external torque exceeds this threshold. The safe joint mechanism enables a robot manipulator to guarantee positioning accuracy and collision safety, and which is simple to install between an actuator and a robot link without a significant change in the robot's design.**

I. Introduction

Because robots work in human environments, safety issues related to physical human-robot interaction have become increasingly important. Therefore, several types of safe robot arms have been proposed to improve collision safety between humans and robots.

A safe robot arm can be achieved by either a passive or active compliance system. In an actively compliant arm, a collision is detected by various types of sensors, and the arm stiffness is lowered by appropriate control of the joint motors [1][2]. Since the active compliance-based approach involves sensing and actuation in response to dynamic collision, it suffers from relatively low bandwidth unless sophisticated and expensive sensors and controllers are used. Furthermore, the installation of a sensor and actuator in the robot arm often leads to high cost, an increase in system size and weight, possible sensor noise, and actuator malfunction.

In contrast, a robot arm based on passive compliance is usually composed of entirely mechanical elements, such as a spring and a flexible link, which can absorb an excessive collision force. Since this approach does not use any sensor or actuator, it can provide fast and reliable responses even for dynamic collision. Several mechanisms have been developed to achieve safety using the passive compliance method.

A mechanical impedance adjuster with a variable spring and an electromagnetic brake was developed in [3]. A programmable passive compliance-based shoulder mechanism using an elastic link was proposed in [4]. A variable stiffness unit with motors, two rings that consist of arc-shaped magnets, and a linear guide was suggested for the safe arm of a service robot in [5]. A variable stiffness actuator with a nonlinear torque transmitting system composed of a spring and a 4-bar mechanism was developed in [6]. A compliance method in the drive system, which mechanically decouples the heavy actuator inertia from the link inertia, was also introduced in [7].

A spring is by far the most popular mechanical element for shock absorption. However, the soft spring used at the joint of a robot arm results in positioning inaccuracy because it operates even for small external forces which do not require shock absorption. This inaccuracy is often made worse by undesirable oscillations caused by the elastic behavior of the spring. Although a stiff spring can provide high positioning accuracy for a robot arm, its capability of shock absorption is much lower than a soft spring, thereby giving a higher probability of injury upon collision with humans. Therefore, an ideal safe manipulator would exhibit very low stiffness when subjected to a collision force capable of causing human injury, but would otherwise maintain a very high stiffness.

In our previous research, this ideal feature was realized by a novel design of a safe link mechanism (SLM) and the safe joint mechanism (SJM-I, II) composed of only passive mechanical elements [8][9][10]. However, implementation of these safety mechanisms for a robot arm requires a simple and compact design.

This paper presents the third version of the safe joint mechanism (SJM-III), which can be installed at the joint part of the robot arm more easily than our previous safety mechanisms. The SJM-III has only three parts: an inclined link, a slider with rollers, and linear springs. Springs are used to absorb collision force, while the inclined link determines whether or not the external torque can be regarded as safe. This enables the SJM-III to operate only in response to a large

This research was supported by the Center for Autonomous Intelligent Manipulation under the Human Resources Development Program for Convergence Robot Specialists and by the Development of Manipulation Technology for Human-Robot Cooperation funded by the Ministry of Knowledge Economy of Korea.

Jung-Jun Park is with the School of Mechanical Engineering, Korea University, Seoul, Korea (e-mail: hantiboy@korea.ac.kr).

Jae-Bok Song is a Professor in the School of Mechanical Engineering, Korea University, Seoul, Korea (Tel.: +82 2 3290 3363; fax: +82 2 3290 3757; e-mail: jbsong@korea.ac.kr).

external torque. The main contribution of our proposed mechanism is the realization of nonlinear stiffness capability using only simple and low-cost mechanical elements. Without compromising positioning accuracy for collision safety, both features can be achieved simultaneously with the SJM-III. Moreover, the problem of the operating range of the SJM-III can be solved by using mechanical limit switches, thus guaranteeing higher collision safety.

The rest of the paper is organized as follows. The operational principle of the SJM-III is discussed in detail in Section II. Section III presents a further description of the prototype model of the SJM-III. Various experimental results for both static and dynamic collisions are provided in Section IV. Finally, Section V presents conclusions and future work.

II. Operational Principle of the Safe Joint Mechanism-III

To simultaneously achieve collision safety and positioning accuracy of a robot arm, we need a nonlinear stiffness mechanism whose stiffness remains very high when the external torque acting on the joint of a manipulator is within the range of normal operation, but drops rapidly when the external torque exceeds a certain level due to collision with the object. In this study, an inclined link equipped with a pre-compressed spring is exploited to achieve this nonlinear stiffness feature.

A. Positioning Accuracy

Consider an inclined link which rotates around O_1 and contacts a roller mounted on the slider shown in Fig. 1. An appropriate force F acting on the slider in the x-axis direction can maintain static equilibrium against the external torque T_{ex} exerted on the link, as shown in Fig. 1(a).

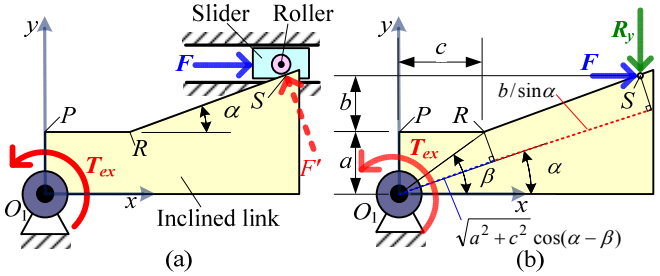

Fig. 1. (a) Inclined link in contact with slider and roller, and (b) free body diagram of inclined link.

From the equation of closure of the mechanism shown in Fig. 1(b), the relationship between T_{ex} and F, which depends on the angle of inclination α, can be obtained by

$$T_{ex} = \left(\sqrt{a^2 + c^2} \frac{\cos(\alpha - \beta)}{\sin \alpha} + \frac{b}{\sin^2 \alpha} \right) F \qquad (1)$$

where the parameters a, b, c and β are defined in Fig. 1(b).

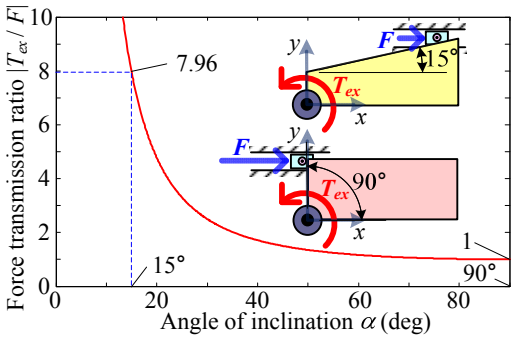

Fig. 2. Ratio of external torque and force as a function of angle of inclination, when a=0.5, b=0.5, and c=0.

Figure 2 shows that the ratio of external torque to force diverges rapidly to positive infinity as α approaches 0° when $a = b = 0.5$ and $c = 0$. For example, if the angle of inclination is set to 15°, the force transmission ratio is almost 8 times that of the angle of 90°. Therefore, even a very small force can make this mechanism statically balanced against a very large external toque using the angle of inclination of the link.

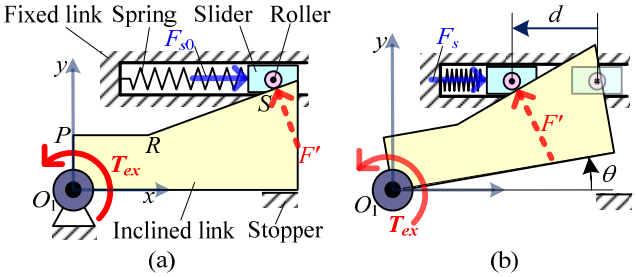

Fig. 3. Nonlinear stiffness mechanism consisting of an inclined link with a pre-compressed spring. (a) Zero configuration, and (b) general configuration.

To generate the force F required to maintain static equilibrium, a pre-compressed spring was installed between the fixed link and the slider which can move in the x-axis direction, as shown in Fig. 3(a). The roller connected to the slider contacts the inclined plane of the link. The stopper is used to prevent the clockwise rotation of the inclined link at the initial position. Therefore, this mechanism can maintain static equilibrium even when only the spring force is applied to the inclined link without the external torque.

Consider a situation in which the external torque T_{ex} is forced to act on the inclined link. Due to the spring force caused by spring compression, the slider cannot move to the left until the external torque exceeds a certain threshold which is large enough to move it to the left. The external torque required to initiate movement of the slider is defined as the threshold torque T_{th}. From Eq. (1), T_{th} is described as

$$T_{th} = \left(\sqrt{a^2 + c^2} \frac{\cos(\alpha - \beta)}{\sin \alpha} + \frac{b}{\sin^2 \alpha} \right) k s_0 \qquad (2)$$

where k is the spring constant and s_0 is the length of the initial spring compression.

Although a spring of small capacity is installed, a small angle of inclination can generate the large threshold torque for this mechanism. A robot arm with this mechanism can maintain high stiffness to accurately handle a payload, thereby generating external torque below the threshold torque and providing positioning accuracy in normal operation.

B. Collision Safety

In this section, the nonlinear stiffness of this mechanism is described. It is assumed that this inclined link rotates counterclockwise (CCW), and thus pushes the slider in the direction of compressing the spring as shown in Fig. 3(b). From the principle of virtual work, the relation between external torque T_{ex} and spring force F_s according to the angular displacement of inclined link θ, which can maintain the static equilibrium of this mechanism, is obtained by

$$T_{ex} = \frac{\delta d}{\delta \theta} F_s = \frac{(1+\tan^2\alpha)(a+b)+(c\tan\alpha - a)(\cos\theta - \sin\theta\tan\alpha)}{(\sin\theta+\cos\theta\tan\alpha)^2} F_s \tag{3}$$

where δd and $\delta\theta$ are the virtual displacements of the slider and the inclined link, respectively. From the equation of closure of this mechanism shown in Fig. 3(b), we obtain

$$F_s = k(s_0 + d) \tag{4a}$$

$$d = c + \frac{b}{\tan\alpha} - \frac{(a+b)(\cos\theta - \sin\theta\tan\alpha) + c\tan\alpha - a}{\sin\theta + \cos\theta\tan\alpha} \tag{4b}$$

For example, when $k = 4$ kN/m, $s_0 = 20$ mm, $a = 11$ mm, $b = 7$ mm, $c = 15$ mm, and $\alpha = 25°$, the external torque and the spring force for static equilibrium of this mechanism as a function of angular displacement of the inclined link are plotted in Fig. 4(a). As the angular displacement θ increases, F_s acting on the slider increases because the spring is further compressed. However, T_{ex} for the equilibrium of this mechanism decreases since the contact angle between the inclined link and the roller increases continuously, as shown in Fig. 3(b).

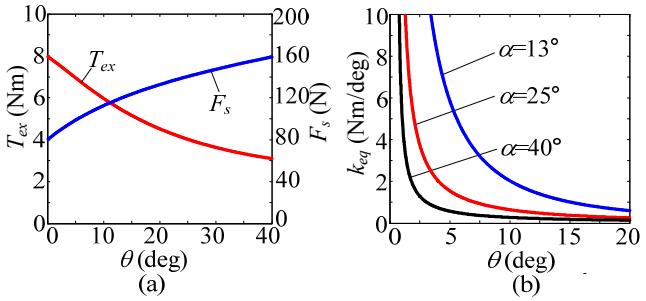

Fig. 4. (a) External torque and spring force versus angular displacement, and (b) equivalent stiffness of nonlinear stiffness mechanism as a function of angular displacement.

From Eq. (3), the equivalent stiffness k_{eq} of this mechanism can be given by

$$k_{eq} = \frac{T}{\theta} = \frac{F_s}{\theta}\frac{(1+\tan^2\alpha)(a+b)+(c\tan\alpha - a)(\cos\theta - \sin\theta\tan\alpha)}{(\sin\theta+\cos\theta\tan\alpha)^2} \tag{5}$$

k_{eq} is kept very high for small values of θ, but quickly drops as θ increases as shown in Fig. 4(b). Furthermore, as the angle of inclination is increased, a lower stiffness for the same angular displacement can be obtained, thereby resulting in relatively easy movement of the slider. However, as the angle of inclination increases, the threshold torque decreases as shown in Fig. 2, so high positioning accuracy cannot be achieved.

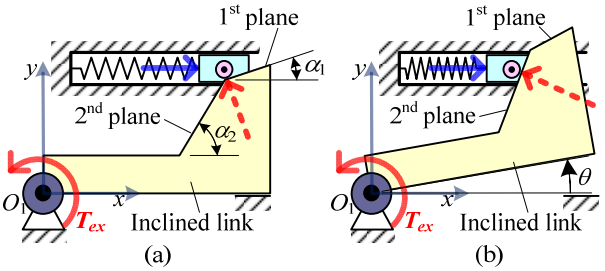

Fig. 5. Inclined link composed of two angles of inclination. (a) Initial static equilibrium, and (b) general motion.

To mitigate this problem, we propose an inclined link composed of two inclined planes which have different angles as shown in Fig. 5. At the initial static equilibrium condition, the roller contacts the first inclined plane whose angle is small, so large threshold torque can be achieved. However, as the link starts rotating, the stiffness abruptly drops because the external torque is transmitted from the second inclined plane with a large angle to the slider with a spring.

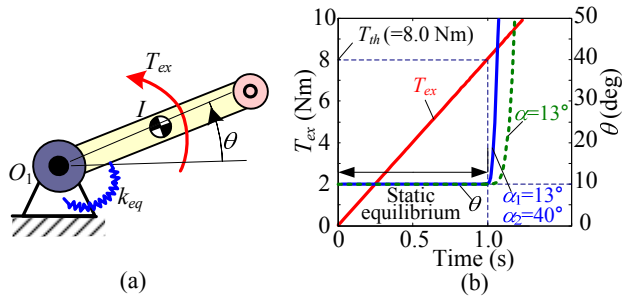

Fig. 6. Dynamic analysis of the nonlinear stiffness mechanism. (a) Simple model, and (b) external torque and angular displacement of inclined link versus time.

To analyze the dynamic motion of the proposed mechanism as shown in Fig. 6(a), we modeled a 1 degree-of-freedom (DOF) link equipped with an equivalent spring whose stiffness was obtained from Eq. (5). In this analysis, $a = 11$ mm, $b = 7$ mm, $c = 15$ mm, $\alpha_1 = 13°$, $\alpha_2 = 40°$, $k = 4$ kN/m, and $s_0 = 20$ mm.

Until the external torque increases to 8.0 N·m, which is below the threshold torque, static equilibrium of the mechanism can be maintained because the link does not move at all, as shown in Fig. 6(b). However, as the external torque $T_{ex}(t)$ increases above the threshold torque, static equilibrium cannot be maintained and the link starts rotating. Since the equivalent stiffness of the mechanism (k_{eq} in Fig. 4(b)) quickly decreases according to rotation of the link, the mechanism behaves as a soft spring. Furthermore, Fig. 6(b) shows that in the case of an inclined link with two different angles of inclination (α_1 = 13° and α_2 = 40°), the angular displacement of the link increases more rapidly than in the case of one angle of inclination (α = 13°). As a result, the proposed mechanism can realize the nonlinear stiffness required for both collision safety and positioning accuracy.

III. Robot Arm with Safe Joint Mechanism-III

A. Prototype Modeling of SJM-III

The nonlinear stiffness mechanism described conceptually in the previous section was used in a new safe joint mechanism (SJM-III). SJM-III consists of an inclined link, linear springs, a base plate, and a slider with rollers, as shown in Fig. 7(a). The inclined link is rotated around a shaft fixed at the base plate. The slider can translate relative to the base plate by means of a linear guide in which friction can be significantly reduced. Two rollers which contact the inclined link are arranged symmetrically so that the external torque applied in both directions can be absorbed. The inclined link to which the external torque is applied exerts force on the roller, and the slider connected to the roller is forced to move in the direction of the compressing springs.

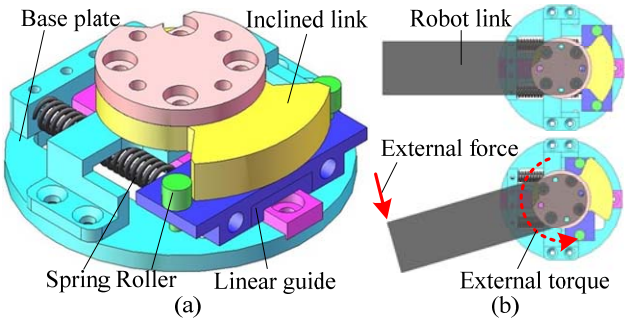

Fig. 7. Prototype model of SJM-III. (a) 3-D computer-aided design (CAD) model, and (b) operation of SJM-III.

If the springs of the SJM-III are fully compressed up to the limit of the operating range and thus the inclined link can no longer rotate, the stiffness of the SJM abruptly increases so it can no longer absorb a collision force. To cope with this problem, mechanical limit switches were installed at the inclined link so that collision can be detected. As shown in Fig. 8(a), to recognize the direction of operation, two limit switches were installed in contact with the inclined link which has two layers of different shape.

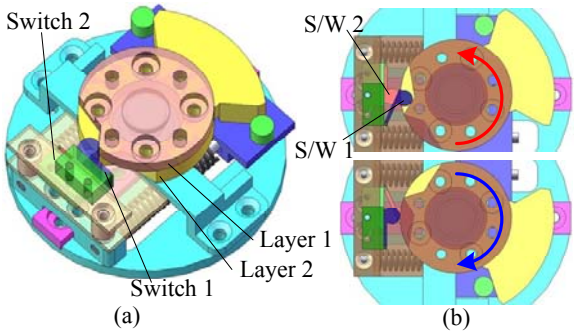

Fig. 8. SJM-III with mechanical limit switches. (a) Zero configuration, and (b) operation of switches.

For example, if static equilibrium of the SJM-III is maintained, all switches are kept on. For CCW rotation, switch 1 turns off and switch 2 stays on as shown in Fig. 8(b), and vice versa.

B. Construction of SJM-III Prototype

The prototype of the SJM-III was constructed as shown in Fig. 9(a). The size of the SJM is ϕ70 x 22 mm, and its weight is 100 g. Most components are made of duralumin which can endure the shock exerted on the SJM-III. The base plate was fixed to a speed reducer with a high gear ratio like the harmonic drive, and the inclined link was connected to the robot link. Therefore, motor torque is transmitted from the speed reducer to the robot link via the SJM-III.

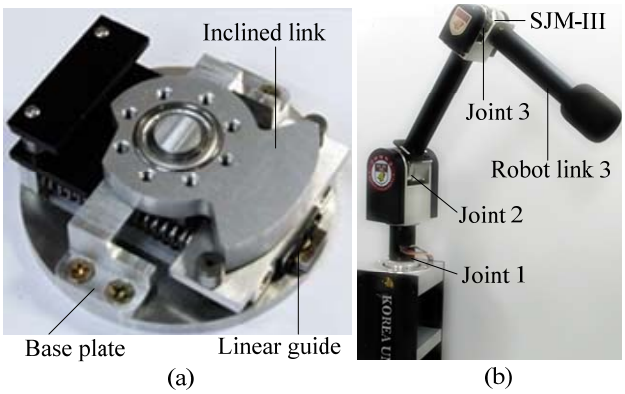

Fig. 9. Prototype of SJM-III. (a) Isometric view, and (b) robot arm with SJM-III.

The SJM-III was installed at joint 3 of the 3 DOF robot arm shown in Fig. 9(b). Therefore, the SJM should be designed in consideration of the weight of the robot link and the weight of the payload. To obtain a different threshold torque of the SJM-III according to the direction of rotation, the initial angle of the upper part of the inclined link was set to 13° and the initial angle of the lower part of the inclined link was set to 25°, as shown in Fig. 10. As a result, the threshold torque in a CW direction was 5.3 N·m, and the threshold torque in a CCW direction was 8 N·m.

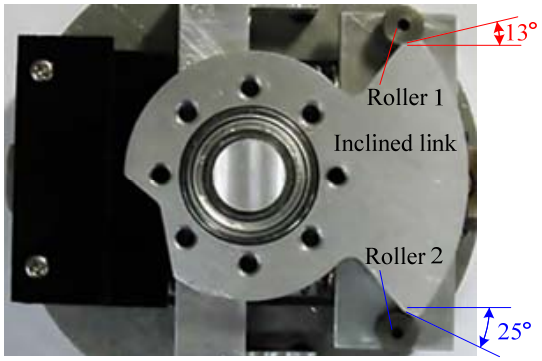

Fig. 10. Non-symmetric inclined link of SJM-III.

IV. Experiments for Safe Joint Mechanism-III

A. Experimental Setups

To conduct various experiments using the SJM-III, a 3 DOF robot arm equipped with the SJM-III was constructed as shown in Fig. 9(b). The lengths and weights of robot link 1, robot link 2, and robot link 3 are 0.25 m, 0.4 m, and 0.4 m, and 2.9 kg, 1.3 kg, and 0.5 kg, respectively. Most components were made of duralumin which could endure the collision force exerted on the robot arm. The collision force was measured by a force/torque sensor. The displacement of the SJM-III was measured by an extra encoder attached to joint 3. The sampling time of the controller of this robot arm was 1 ms for the actuation of motors and processing of switch signals.

B. Experimental Results

In our experiment for static collision, the end-point of the robot arm was initially positioned to barely touch a fixed plate, and the joint torque provided by the motor was slowly increased. The static collision force between the robot and the fixed plate was measured by a force/torque sensor. As shown in Fig. 11, experiments were conducted for the robotic arms with and without the SJM-III. The robot link was forced to rotate in both the direction of gravity and the opposite direction.

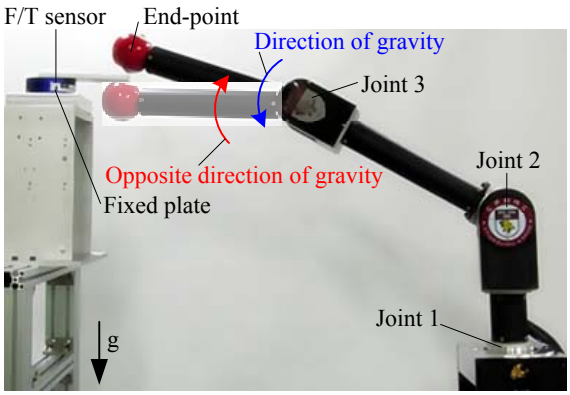

Fig. 11. Experimental setup for static collision.

The robot arm without the SJM-III delivered a contact force which increased to 60 N at the fixed plate due to high stiffness of the speed reducer. However, for both directions, contact forces of up to 20 N and 13.5 N, respectively, were transmitted to the fixed plate of the robot arm with the SJM-III as shown in Fig. 12(a). Although the motor continually rotated after collision, contact forces decreased to about 10 N. A contact force above pain tolerance (50 N [11]) did not occur because the excessive force was absorbed by the SJM-III.

As shown in Fig. 12(b), virtually no displacement of the SJM-III occurred in the opposite direction of gravity when external torque due to the contact force was below 8 N·m. Therefore, the robot arm with the SJM-III can accurately handle a payload of up to approximately 1.5 kg (15 N) as though it had a speed reducer with a high gear ratio. However, as the external torque increased above the threshold torque, the stiffness of the SJM-III quickly diminished. Thus, the SJM-III provided high positioning accuracy of the robot arm in normal operation, and guarantees safe human-robot contact by absorbing a contact force above 50 N in a collision.

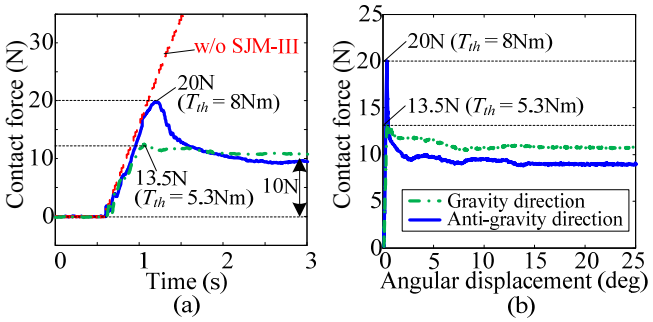

Fig. 12. Experimental results for static collision for robot arm. (a) Collision force versus time with and without SJM-III, and (b) collision force versus angular displacement of the SJM-III.

Next, dynamic collision experiments were conducted for the robot arm equipped with and without the SJM-III. A robot link rotating at an angular velocity of 208 °/s, which corresponds to an end-point velocity of 2 m/s, was forced to collide with a fixed urethane ball. The collision force between the wall and the robot link was measured by an F/T sensor mounted on the ball. For the robot arm with the SJM-III, two kinds of safety strategies were applied when the collision was detected by switch signals. Strategy 1 is an emergency stop of the actuators of the robot arm as soon as a collision is detected [2]. Strategy 2 is a reflexive motion which means that an actuator rotates in the opposite direction as soon as a collision is detected.

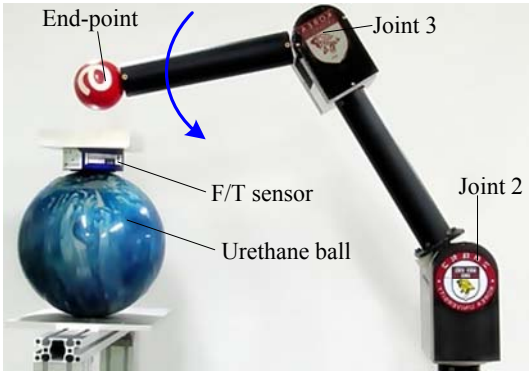

Fig. 13. Experimental setups for dynamic collision.

The experimental results are shown in Fig. 13. For a dynamic collision of the robot arm without the SJM-III, the collision force reached a peak value of 391 N, which is above the fracture tolerance of the nasal bone (345 N, as reported in [12]). Therefore, collision with the robot arm without the SJM-III has sufficient force to cause injury to a human.

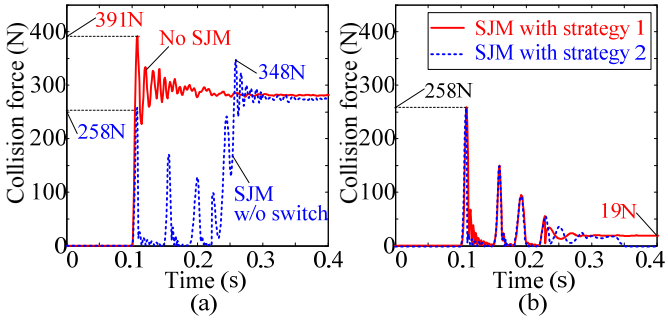

Fig. 13. Experimental results on dynamic collision. (a) No SJM-III and SJM-III without switch, and (b) SJM-III with strategies 1 and 2.

In the case of the robot arm with the SJM-III, when no strategy was applied, the first peak value of the collision force increased to 258 N, which was much less than the force without the SJM-III. However, when the actuator continuously rotated after the collision, the second collision force reached 348 N due to the limit of the operating range of the SJM-III. Next, when strategy 1 (emergency stop) was applied, the collision force reached 258 N, and immediately dropped to 19 N due to the operation of the SJM-III. When strategy 2 (reflexive motion) was applied, the peak value of the collision force reached 258 N, but immediately after collision no collision force was delivered to the urethane ball. As a result, the robot arm with the SJM-III provides much higher safety for human-robot contact than the arm without the SJM-III. Furthermore, if the safety strategies are applied, the problem of the operating range of the SJM-III can be solved.

V. Conclusions

In this study, the third version of a safe joint mechanism (SJM-III) was proposed for collision safety. SJM-III has smaller size, lighter weight, and lower cost than the previous SJMs. A robot arm equipped with the SJM-III can maintain very high stiffness up to a preset threshold torque, and provides a very low stiffness above the threshold. From our analysis and experiments, the following conclusions are drawn:

1) The stiffness of the robot manipulator abruptly drops if the external torque to the SJM-III exceeds the pre-determined threshold torque. Therefore, collision safety can be achieved even for a high-speed dynamic collision.

2) High stiffness of the robot arm can be maintained for external torque that is lower than the threshold torque. Therefore, positioning accuracy can be achieved in normal operation.

4) The SJM-III can be designed in consideration of gravity compensation by setting different threshold torques in both directions of rotation.

5) Since a collision is detected by limit switches, a robot arm with the SJM-III can react to the collision. Therefore, the problem with the limit of the operating range of the SJM-III can be solved, thus maintaining the robot arm in the safe region.

6) Since the SJM-III is simple enough to be installed between an actuator and a robot link, it can be applied to any type of robot arm without much modification of the robot.

Currently, simpler and more lightweight safe joint mechanisms are under development so that several SJMs may be used simultaneously in the robot arm without a significant increase in cost and weight.

References

[1] K. K. Gupta, "Fast Collision Avoidance for Manipulator Arms: A Sequential Search Strategy," *IEEE Transactions on Robotics and Automation*, Vol. 6, No. 5, pp. 522-532, 1990.10.

[2] A. De Luca, A. Albu-Schaffer, S. Haddadin and G. Hirzinger, "Collision detection and safe reaction with the DLR-III lightweight manipulator arm," *Proc. of the IEEE/RSJ International Conference on Intelligent Robots and System*, pp. 1623-1630, 2006.

[3] T. Morita and S. Sugano, "Development and evaluation of seven DOF mia arm," *Proc. of the IEEE International Conference on Robotics and Automation*, pp. 462-467, 1997.

[4] M. Okada, Y. Nakamura and S. Ban, "Design of programmable passive compliance shoulder mechanism," *Proc. of the IEEE International Conference on Robotics and Automation*, pp.348-353, 2001.

[5] J. Choi, S. Park, W. Lee, and S. Kang, "Design of a Robot Joint with Variable Stiffness," *Proc. of the IEEE International Conference on Robotics and Automation*, pp. 1760-1765, 2008.

[6] R. Schiavi, G. Grioli, S. Sen and A. Bicchi, "VSA-II: a Novel Prototype of Variable Stiffness Actuator for Safe and Performing Robots Interacting with Humans," *Proc. of the IEEE International Conference on Robotics and Automation*, pp. 2171-2176, 2008.

[7] M. Zinn, O. Khatib, B. Roth and J. K. Salisbury, "A new actuation approach for human-friendly robot design," *International Journal of Robotics Research*, vol. 23, no. 4/5, pp. 379-398, 2005.

[8] J.-J. Park, B.-S. Kim, J.-B. Song and H.-S. Kim, "Safe Link Mechanism based on Nonlinear Stiffness for Collision Safety," *Mech. Mach. Theory* , Vol. 43, No. 10, pp. 1332-1348, 2008.10.

[9] J.-J. Park, Y.-J. Lee, J.-B. Song and H.-S. Kim, "Safe Joint Mechanism based on Nonlinear Stiffness for Safe Human-Robot Collision," *Proc. of the IEEE International Conference on Robotics and Automation*, pp. 2177-2182, 2008.

[10] J.-J. Park, H.-S. Kim, and J.-B. Song, "Safe Robot Arm with Safe Joint Mechanism using Nonlinear Spring System for Collision Safety," *Proc. of the IEEE International Conference on Robotics and Automation*, pp. 3371-3376, 2009.

[11] Y. Yamada, Y. Hirasawa, S.Y. Huang and Y. Umetani, "Fail-safe human/robot contact in the safety space," *IEEE International Workshop on Robot and Human Communication*, pp. 59-64, 1996.

[12] A. M. Nahum, "Impact studies of Facial Bones and Skull." SAE Paper No. 720965, *Sixteenth Stapp Car Crash Conference*, Nov. 8-10, 1972.